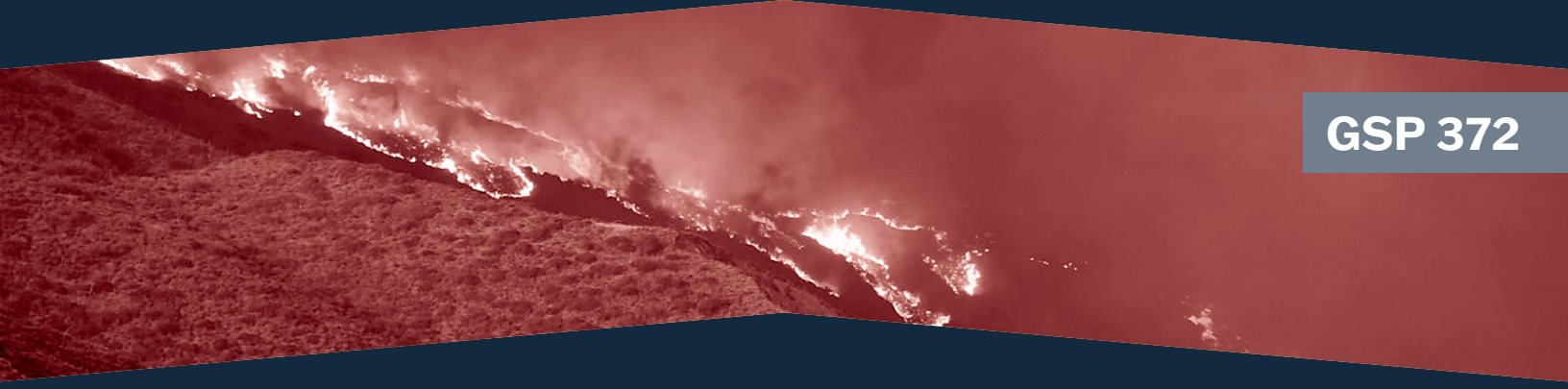


GSP 372

Geo-Extreme 2025



Different Climates and the Coastal Zone



Selected Papers from Geo-Extreme 2025
Long Beach, California • November 2–5, 2025

EDITED BY

Christopher L. Meehan, Ph.D., P.E., BC.GE;
James A. McKelvey III, Ph.D., P.E., BC.GE;
Adda Athanasopoulos-Zekkos, Ph.D.;
Miguel A. Pando, Ph.D., P.Eng.; Nina Stark, Ph.D.;
and Ming Xiao, Ph.D., P.E., BC.GE

ASCE

G-I ASCE GEO-INSTITUTE

GEOTECHNICAL SPECIAL PUBLICATION NO. 372

GEO-EXTREME 2025

DIFFERENT CLIMATES AND THE COASTAL ZONE

SELECTED PAPERS FROM GEO-EXTREME 2025

November 2–5, 2025
Long Beach, California

SPONSORED BY

The Geo-Institute
of the American Society of Civil Engineers

EDITED BY
Christopher L. Meehan, Ph.D., P.E., BC.GE
James A. McKelvey III, Ph.D., P.E., BC.GE
Adda Athanasopoulos-Zekkos, Ph.D.
Miguel A. Pando, Ph.D., P.Eng.
Nina Stark, Ph.D.
Ming Xiao, Ph.D., P.E., BC.GE

Published by the American Society of Civil Engineers

Published by American Society of Civil Engineers
1801 Alexander Bell Drive
Reston, Virginia, 20191-4382
www.asce.org/publications | ascelibrary.org

Any statements expressed in these materials are those of the individual authors and do not necessarily represent the views of ASCE, which takes no responsibility for any statement made herein. No reference made in this publication to any specific method, product, process, or service constitutes or implies an endorsement, recommendation, or warranty thereof by ASCE. The materials are for general information only and do not represent a standard of ASCE, nor are they intended as a reference in purchase specifications, contracts, regulations, statutes, or any other legal document. ASCE makes no representation or warranty of any kind, whether express or implied, concerning the accuracy, completeness, suitability, or utility of any information, apparatus, product, or process discussed in this publication, and assumes no liability therefor. The information contained in these materials should not be used without first securing competent advice with respect to its suitability for any general or specific application. Anyone utilizing such information assumes all liability arising from such use, including but not limited to infringement of any patent or patents.

ASCE and American Society of Civil Engineers—Registered in U.S. Patent and Trademark Office.

Photocopies and permissions. Permission to photocopy or reproduce material from ASCE publications can be requested by sending an e-mail to permissions@asce.org or by locating a title in ASCE's Civil Engineering Database (http://cedb.asce.org) or ASCE Library (http://ascelibrary.org) and using the "Permissions" link.

Errata: **Errata, if any, can be found at https://doi.org/10.1061/9780784486528**

Copyright © 2025 by the American Society of Civil Engineers.
All Rights Reserved.
ISBN 978-0-7844-8652-8 (PDF)
Manufactured in the United States of America.

Preface

The Embankments, Dams, and Slopes (EDS) Technical Committee of the ASCE Geo-Institute organized a timely and interesting specialty conference in 2021 in Savannah, Georgia, entitled *Geo-Extreme 2021: Geotechnical Engineering for Extreme Events*. This 2021 conference was intended as an inaugural specialty conference, and the beginning of a series of planned conferences organized by the EDS committee seeking to address the many societal challenges that are posed by extreme events such as: earthquakes, hurricanes, landslides, debris flows, wildfires, tornadoes, extreme rainfall events, blizzards, and other extreme loading events caused by changing weather patterns. This 2021 conference built on three previous slope stability related conferences that were organized by the EDS committee, two in 1966 and 1992 at the University of California at Berkeley and one in 2013 in San Diego. Strong impetus for that meeting was provided by a number of very significant extreme events in the United States, starting with Hurricanes Katrina in 2005 and Sandy in 2012 followed by Hurricanes Harvey, Irma, and Maria in 2017, and then Hurricanes Laura, Delta, and Zeta in 2020, which all caused widespread damage to communities at large, and particular damage to natural slopes and engineered structures that are the purview of the EDS Committee.

Since the 2021 conference, the onslaught of extreme loading events in the United States has continued unabated, with significant loss of life and severe financial consequences to communities that are unprecedented. The impact of major hurricanes including Ian, Ida, Idalia, Helene, and Milton has been strongly felt in coastal communities but also ranging far inland. Extreme rainfall and flood events have caused damages averaging in excess of a billion dollars annually, particularly in California. Severe storms, winds, and flooding also battered Kentucky heavily in 2025. Wildfires brought significant destruction and caused numerous deaths in Hawaii's Lahaina fire of 2023, the Smokehouse Creek fire in Texas and Oklahoma in 2024, and in California with the Park Fire in 2024 and wildfires in Southern California in 2025. The 2023 fire season was also particularly significant in Canada, which saw 45,700,000 acres of land burn across ten provinces and three territories.

Following these extreme events, the EDS Committee has proposed and organized the current specialty conference, *Geo-Extreme 2025: Geotechnical Engineering for Extreme Events*. The goal of this conference is to continue to draw attention to the pressing problems posed by extreme events, and to identify the critical role that geotechnical engineers and the civil engineering profession as a whole can play in mitigating the effects of these events, both before they occur, as well as after – that is, "building back safer" in a way that benefits both the built and natural environments.

Historical records show that the number of billion-dollar extreme events are on the rise. Mitigating the consequences of future extreme events requires geo-professionals taking timely actions, including evaluation of existing earthen structures, design and construction of protective structures in areas where an increased probability of damage is expected, refinement of existing geotechnical designs, and development of new adaptive measures and risk assessment tools. To achieve these objectives, the Geo-Extreme 2025 conference will comprise a multi-disciplinary forum between geotechnical engineers and other professionals from related disciplines, such as scientists, various

© ASCE

types of engineers, emergency managers, resilience and sustainability investigators, insurance experts, and policy makers, to provide solutions that properly cope with and address the wide variety of extreme events that can occur.

There are five volumes containing the full collection of papers presented at Geo-Extreme 2025: Geotechnical Engineering for Extreme Events, which was held on November 2-5, 2025, in Long Beach, California. These five volumes are subtitled: (1) Remote Sensing, Instrumentation, Big Data, and Decision Making, (2) Geotechnical Earthquake Engineering, (3) Civil Infrastructure, Geomaterials, and Case Histories, (4) Different Climates and the Coastal Zone, and (5) Permafrost, Wildfires, and Other Emerging Challenges in Geotechnical Engineering, respectively. These five volumes include over 130 contributions that span 25 subtopic areas of the conference, as noted in the subsequent tables of contents for each volume. Each of the five volumes are Geotechnical Special Publications (GSPs), containing papers that were reviewed in accordance with ASCE GSP standards. Each paper was subjected to technical review by two or more independent peer reviewers, and publication required concurrence by at least two peer reviewers.

The Editors gratefully acknowledge the immeasurable contributions of the countless individuals who made Geo-Extreme 2025 and these published proceedings possible, especially the reviewers, session chairs, organizing committee members, and ASCE staff listed in the acknowledgements.

The Proceedings Editors,

Christopher L. Meehan, Ph.D., P.E., BC.GE, F.ASCE, University of Delaware
James A. McKelvey, III, Ph.D., P.E., BC.GE, F.ASCE, Earth Engineering Incorporated
Adda Athanasopoulos-Zekkos, Ph.D., M.ASCE, University of California, Berkeley
Miguel A. Pando, Ph.D., P.Eng., M.ASCE, Drexel University
Nina Stark, Ph.D., M.ASCE, University of Florida
Ming Xiao, Ph.D., P.E., BC.GE, F.ASCE, Pennsylvania State University

© ASCE

Acknowledgments

The conference and its published proceedings would not have been possible without the diligent, coordinated effort of numerous people, especially the reviewers who provided detailed feedback on papers and the session chairs who made decisions and provided editorial assistance on selected topics. The editorial team is also profoundly grateful to Dr. Daniel Pradel and Dr. Navid Jafari (Conference Co-Chairs), the Technical Program Committee (listed below), Mr. Brad Keelor, Ms. Aurora Phlegar, and the ASCE publications team for their crucial roles in the production of these proceedings.

Geo-Extreme 2025 Conference Program Committee

Conference Co-Chairs

- Daniel Pradel, Ph.D., P.E., M.ASCE, *Ohio State University*
- Navid H. Jafari, Ph.D., M.ASCE, *Texas A&M University*

Technical Program Committee

- Timothy D. Stark, Ph.D., P.E., BC.GE, F.ASCE, *University of Illinois at Urbana-Champaign*
- James A. McKelvey, III, Ph.D., P.E., BC.GE, F.ASCE, *Earth Engineering Incorporated*
- Jeremy Varner, P.E., M.ASCE, *Federal Energy Regulatory Commission*
- Nazli Yesiler, Ph.D., A.M.ASCE, *California Polytechnic State University, San Luis Obispo*
- Ghada Ellithy, Ph.D., P.E., M.ASCE, *Embry-Riddle Aeronautical University*
- Stefan G. Flynn, P.E., M.ASCE, *US Army Corps of Engineers, Rock Island District*

Proceedings Editors

- Christopher L. Meehan, Ph.D., P.E., BC.GE, F.ASCE, *University of Delaware*
- James A. McKelvey, III, Ph.D., P.E., BC.GE, F.ASCE, *Earth Engineering Incorporated*
- Adda Athanasopoulos-Zekkos, Ph.D., M.ASCE, *University of California, Berkeley*
- Miguel A. Pando, Ph.D., P.Eng., M.ASCE, *Drexel University*
- Nina Stark, Ph.D., M.ASCE, *University of Florida*
- Ming Xiao, Ph.D., P.E., BC.GE, F.ASCE, *Pennsylvania State University*

© ASCE

Contents

Impacts from Weather and Climate

A Rapid Heatwave Prediction and Delivery System through Automatic Generation of 3D Urban Models and Automated Execution of Microclimate Simulations 1
Toshihiro Kameda, Kazuya Honda, Keigo Matsuda, Yuya Kurihara, Moe Someya, Hitoshi Nakase, Toru Sugiyama, and Kazuhiko Igata

Quantitative Evaluation Methods of Ash and Cement Concrete Powder: CO_2 Fixation Reactions 9
Shun Kawabe, Haruya Suzuki, Sota Murase, Hideo Komine, and Daichi Ito

Harnessing Climate Data for Climate-Resilient Pavement Deterioration Modeling 19
Wei Sun, Meisam Khorshidi, Mohamad Elshaer, Eshan Dave, and Jo Sias

Long-Term Weather-Driven Deterioration of Clay Embankments under a Changing Climate in Los Angeles, California 29
Amr M. Morsy and Emma Varela

Modelling the Spatial Correlation of Tropical Cyclone Wind Field Residuals 39
Amirreza Mohammadi and Michelle T. Bensi

An Experimental Small-Scale Study of Floating Offshore Wind Turbine Systems: Anchor Failure and Scaling Considerations 48
Brayden Curry and Srikanth S. C. Madabhushi

Rainfall, Erosion, Geohazards, and Landslides

Analyzing Wall Failure in Mud-Capped Dredge Pits along the Louisiana Continental Shelf 57
Omar Alawneh, Navid H. Jafari, Wenqiang Zhang, and Kehui Xu

The Influence of Model Spatial Resolution on Rainfall-Induced Landslide Prediction for a Basin in Utuado, Puerto Rico 67
Mirna Kassem and Dimitrios Zekkos

Case Study of Debris Flow Mitigation—City of Glenwood Springs, Colorado 78
Aliena M. Debelak, Bailey J. Fischer, Roger A. Pihl, and P. G. Ryan Gordon

Assessing the Resiliency of a Highway Slope against Extreme Rainfall Events 90
Fariha Rahman and Sadik Khan

© ASCE

Coastal Soil Properties

Determination of Void Ratio Distribution within a Coastal Soil Sample Using Laboratory Test Methods and Image Analysis of X-Ray CT Scans 100
Siamak Yoosefi, William J. Baker III, and Christopher L. Meehan

Advanced CFD-DEM Analysis of Coastal Sand Dunes under Wave Attack 110
Ekansh Agarwal and Ning Luo

Assessing Spatial Variations in Dynamic Cone Penetration across Bays and Horns on a Cuspate Shoreline 121
Mohamad El Ahmad, Sarah Burghardt, Thomas Mayer, Stephen Adusei, Jonathan Hubler, Nina Stark, and Tian-Jian Hsu

Application of Direct Shear Testing to Assess the Influence of Mangrove Root Structures on the Shear Strength of Coastal Wetlands 130
Mohamed Hassan, Andre Rovai, Hamed Nasiri, Ivan Vargas Lopez, Youssef Mousa, Aaron Meyers, Jorge A. Pineda Gomez, Xiaochen Zhao, Daniel J. Jensen, Annemarie E. Peacock, Anna R. Armitage, Jaime Brinkley, Briana Sebastian, Jacob Berkowitz, Marc Simard, Robert Twilley, and Navid Jafari

Investigating the Driving Mechanisms of a Wetland Tension Crack 141
Brian D. Harris, Aleksandra Ostojic, Jonathan Hubler, Anthony Priestas, Daniel Gallegos, Justin Shawler, and Lenore Tedesco

Coastal Hazards and Mitigation

Full-Scale Testing of Sheet Pile for Storm Surge Wall 151
Guoming Lin and Cheng Lin

Spatiotemporal Variability of Beach Sediment Properties Pre- and Post-Hurricanes Debby and Helene at South Ponte Vedra Beach, Florida 160
Stephen Adusei, Nina Stark, and Noah Evans

Integrated Geotechnical and Geophysical Assessments of Erosion Dynamics in a Chenier Plain Shell Beach following Hurricanes and Seasonal Weather Events 170
Cyrus D. Bahman, Hamed Nasiri, Omar Alawneh, Benjamin A. Fernandez, and Navid H. Jafari

Needs, Opportunities, and Challenges of Pre-, during, and Post-Storm Reconnaissance in Coastal Environments 180
Nina Stark, Michael H. Gardner, Michael Grilliot, Britt Raubenheimer, and J. David Frost

© ASCE

Geotechnical Response of Cheniers to Breakwaters and Hurricanes: A Case Study in Rockefeller Wildlife Refuge.....189
Hamed Nasiri, Omar Alawneh, Navid H. Jafari, and Mohamed O. Hassan

Fragility Analyses of Coastal Slab-on-Grade Foundations Exposed to Storm Surge-Induced Scour.....199
Hiramani Raj Chimauriya, Anand J. Puppala, and Nripojyoti Biswas

© ASCE

A Rapid Heatwave Prediction and Delivery System through Automatic Generation of 3D Urban Models and Automated Execution of Microclimate Simulations

Toshihiro Kameda, Ph.D.[1]; Kazuya Honda, Ph.D.[2]; Keigo Matsuda, Ph.D.[3]; Yuya Kurihara[4]; Moe Someya[5]; Hitoshi Nakase, Ph.D.[6]; Toru Sugiyama, Ph.D.[7]; and Kazuhiko Igata[8]

[1]Institute of Engineering Mechanics and Energy, Univ. of Tsukuba, Tsukuba, Ibaraki, Japan. Email: kameda@kz.tsukuba.ac.jp
[2]Tokyo Electric Power Service Co., Ltd., Tokyo, Japan. Email: kazuya-honda@tepsco.co.jp
[3]Japan Agency for Marine-Earth Science and Technology, Yokosuka, Kanagawa, Japan. Email: k.matsuda@jamstec.go.jp
[4]College of Engineering Systems, Univ. of Tsukuba, Tsukuba, Ibaraki, Japan. Email: s2011059@u.tsukuba.ac.jp
[5]Dept. of Engineering Mechanics and Energy, Graduate School, Univ. of Tsukuba, Tsukuba, Ibaraki, Japan. Email: s2320868@u.tsukuba.ac.jp
[6]Tokyo Electric Power Service Co., Ltd., Tokyo, Japan. Email: nakase@tepsco.co.jp
[7]Japan Agency for Marine-Earth Science and Technology, Yokosuka, Kanagawa, Japan. Email: tsugi@jamstec.go.jp
[8]Tokyo Electric Power Service Co., Ltd., Tokyo, Japan. Email: igata@tepsco.co.jp

ABSTRACT

We developed a system to simulate heatwaves in a 2 km square area with a 5-m resolution, aimed at supporting heatstroke prevention decisions in urban areas with numerous structures. To achieve practical operational speed, the system enables automatic generation of 3D urban models and automated execution of microclimate simulations on parallel computing systems. Furthermore, to facilitate effective decision-making, we implemented a GUI that automatically delivers simulation results and visualizes them in a web browser. For the generation of 3D urban models, we can use not only the current urban data provided in CityGML format but also CAD data and raster data for structures that are not yet constructed. This allows for the use of heatwave simulations as an evaluation tool for appropriately placing new structures in existing urban environments. At the conference, we plan to provide an explanation of the system and present representative results.

INTRODUCTION

Due to the impacts of recent extreme climate change, the risk of heatstroke during summer has been increasing (Japan Meteorological Agency 2024). This is particularly concerning for outdoor events held during the summer, where the risk of heatstroke is significant. To predict the risk of heatstroke, it is necessary to use meteorological models capable of calculations at the microclimate level, considering the influence of buildings and other factors. Starting in April 2025, the Japan World Expo ("Osaka-Kansai Expo") will be held on Yumeshima, an artificial island in Osaka Bay. Approximately 28.2 million visitors are expected to attend the Osaka-Kansai Expo. Since the event period includes summer, heatstroke prevention measures are critical, and the need for risk evaluation is high. Therefore, in this study, we conducted preliminary simulations targeting the Expo venue, Yumeshima. We utilized a multi-scale

© ASCE

atmosphere-ocean coupled model called MSSG (Multi-Scale Simulator for the Geoenvironment), developed by the Japan Agency for Marine-Earth Science and Technology (JAMSTEC). MSSG enables calculations ranging from the global scale to the regional and urban scales, allowing microclimate calculations with resolutions of several meters, incorporating 3D shapes of buildings and tree canopies (Onishi et al. 2019). For microclimate calculations, information on the buildings in the target area (a digital twin of the buildings) is required. However, manually creating input data is impractical in urban areas with numerous buildings. In Japan, the Ministry of Land, Infrastructure, Transport and Tourism has made 3D urban model data (Project PLATEAU) publicly available through the National Land Information Platform. Therefore, in this study, we developed a method to automatically create digital twins for calculations from this data, significantly reducing the effort required for creating digital twins of buildings using Data Processing Platform (DPP) (O-Tani et al. 2022).

Additionally, by automating the processes of generating initial and boundary conditions, performing computations on supercomputers, post-processing, and distributing the results via the Internet, we built a system capable of rapidly providing information to users. By automating the creation of urban models for the target region and utilizing supercomputers, we have developed a system capable of generating weather forecasts for the following day with a resolution of 2 meters within 1 km² areas, based on weather data up to the previous day. This enables automated analysis at a frequency of once per day. To further ensure accuracy, it is crucial to measure, accumulate, and distribute various meteorological data, such as temperature, humidity, wind direction, wind speed, and solar radiation, in a simple and automated manner. By utilizing Long Range Wide Area Network (LoRaWAN) that is a wireless communication standard designed for low power consumption and to cover a range of several kilometers (LoRa Alliance 2020). We established a temperature and humidity data collection system that achieves these goals by simply placing measurement devices at desired locations.

METHOD

Creation of Digital Twin for Buildings. As a data conversion and integration technology, the Institute of Physical and Chemical Research (RIKEN) has developed the Data Processing Platform (DPP). In this study, we created a library that enables PLATEAU data from the Ministry of Land, Infrastructure, Transport and Tourism to be imported into the DPP and output in a format compatible with MSSG microclimate analysis. Using this library, we constructed a digital twin based on PLATEAU data for Osaka City. Figures 1 and 2 show the land use classifications and building heights.

From the constructed digital twin, we extracted a 1 km² region of Osaka Bay's artificial island at a resolution of 2 meters for the simulation. When targeting urban areas in the planning stage, it is necessary to integrate data not included in PLATEAU into the digital twin. In this study, we constructed 3D models by extracting contours from raster drawings and assigning height information to the vertices of these contours. By importing the constructed 3D models into the DPP, we confirmed that integration of raster drawings data into the digital twin is also possible.

Numerical method. To predict the microscale heat environment, we perform large-eddy simulation (LES) of micrometeorology using Multi-Scale Simulator for the Geoenvironment (MSSG). MSSG is capable of running atmospheric simulations covering global, meso- and urban scales. At the urban scales, it works as the LES model coupled with three-dimensional radiative

© ASCE

transfer model, resolving building shapes and tree crowns. The heat stroke risk is evaluated by using the wet-bulb globe temperature (WBGT), computed based on pseudo observation of wet-bulb and globe temperatures. The side boundary data for the LES are given by mesoscale downscaling from the mesoscale forecast data distributed from Japan Meteorological Agency (JMA) because it took more than real time for the time integration of the LES. The microscale prediction can provide the WBGT map in a few meters mesh while it can be deviated from the real situation due to the uncertainty in the JMA forecast data. To reduce the prediction error caused by the uncertainty, the WBGT prediction is improved by observation data from a sensor network arranged around the venue. The air temperature, relative humidity, and WBGT are measured at the sensors. We consider the temperature and relative humidity biases, which are caused by the JMA forecast data and nearly homogeneous in the LES domain, and their nonlinear effect on the WBGT is estimated by minimizing the error between the model prediction and the sensor data.

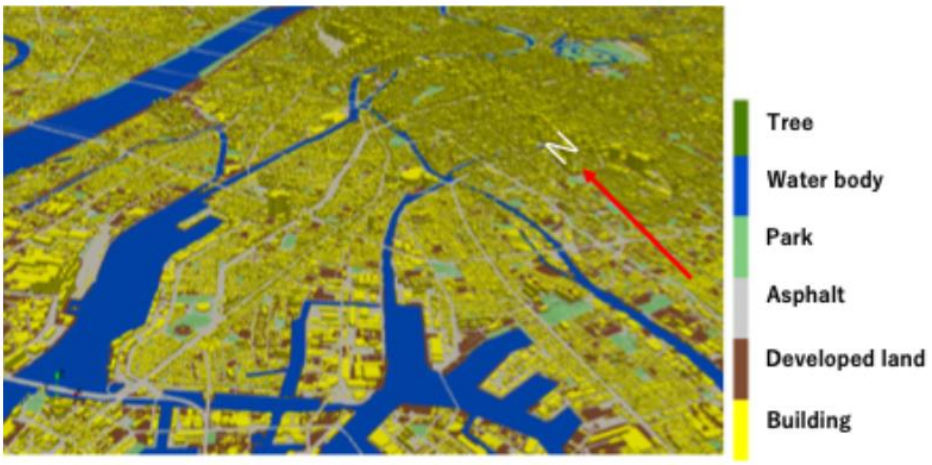


Figure 1. Land use of Osaka City.

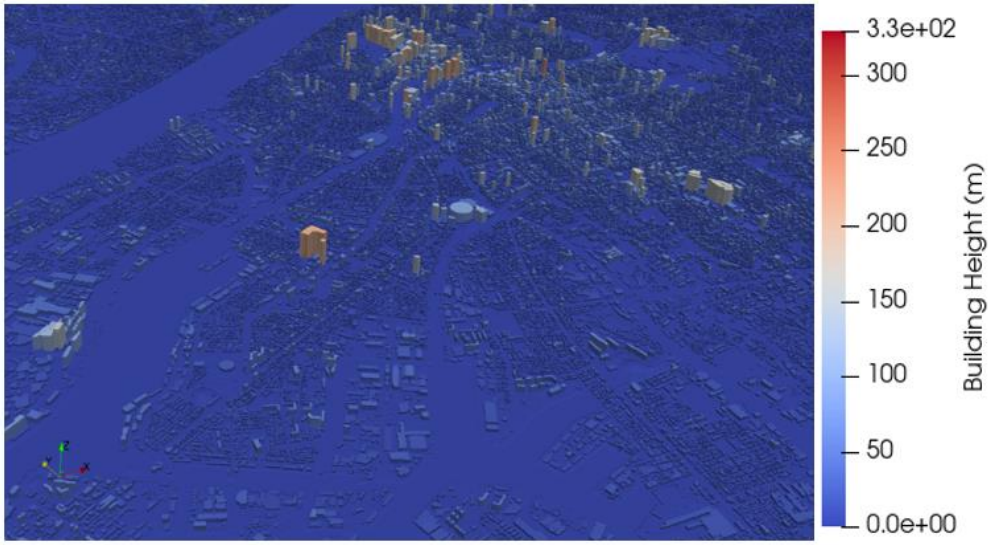


Figure 2. Building height.

© ASCE

Measurement. For the communication method of the sensor network used to collect data, we selected LoRaWAN. Data communication is performed via wireless connections using LoRa modulation between end devices and gateways. The gateway then transfers the data collected from the end devices to a server on the Internet. The gateway placed on the rooftop of a six-story building near the Expo venue is shown in the left side of Figure 3.

LoRaWAN has features such as an open development environment, no licensing requirements, and the ability to connect multiple devices simultaneously. In this study, temperature and humidity are the measurement targets, and a method is employed where three sensors performed simultaneous measurements to detect sensor degradation or failure. Each sensor has been calibrated using a standard thermometer. The developed sensors and end device are presented in the right side of Figure 3.

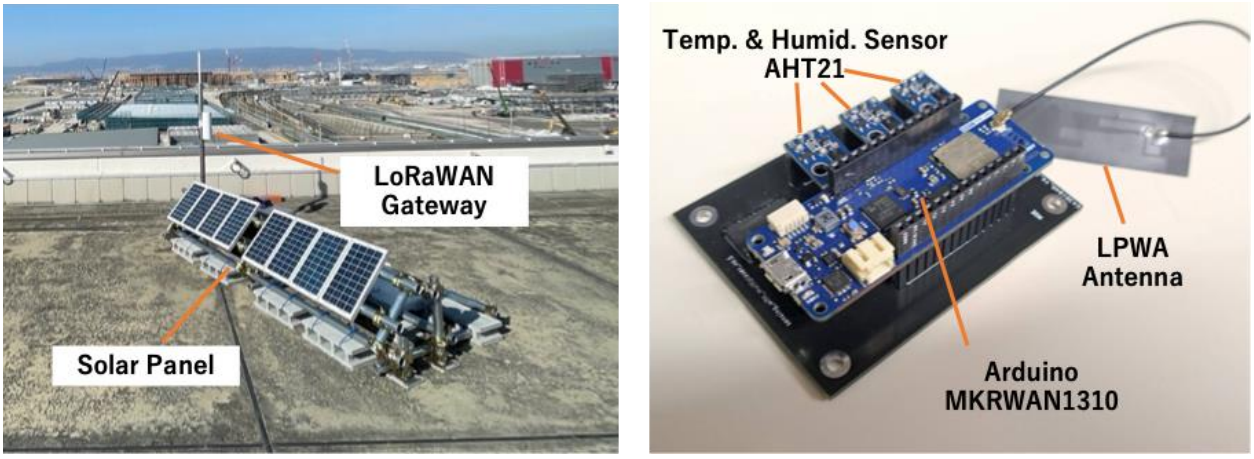


Figure 3. LoraWAN gateway (left) and LoRaWAN end device (right).

Automated Execution. Figure 4 illustrates a system that automatically performs the generation of building data, acquisition of various meteorological data, and microscale weather simulations using MSSG. This system can be configured for periodic execution using cron commands with SCP and SFTP file transfer.

RESULTS AND DISCUSSION.

In the micrometeorological analysis, three levels of mesoscale meteorological simulations, from Nest Levels 0 to 2, were first conducted, as shown on the left side of Figure 5. Next, micrometeorological simulations with building resolution were performed for a 1 km² area outlined in red on the right side of Figure 5. The results of the meteorological analysis at Nest Level 2 (20 km) are shown in Figure 6. Using these results as initial and boundary conditions, micrometeorological simulations with building resolution were conducted based on the automatically constructed digital twin.

A system operation test was conducted as part of the preliminary preparations for actual deployment at the 2025 Expo. The numerical calculations cover the entire Expo site and will be conducted over several hours during which heatstroke prevention measures are necessary. The close-up results of the building-resolution meteorological calculations are presented in Figure 7 and Figure 8. The results of temperature and humidity are presented as examples. The aerial

© ASCE

photo shows the building, and temperature and humidity were measured at the locations near the buildings indicated by red circles in the Figure 7. The upper part of Fig. 8 shows the temperature, and the lower part shows the relative humidity over time for November 11, 2023, from 14:30 to 14:50. Red dots represent measured values, while the blue solid line represents the micrometeorological simulation results.

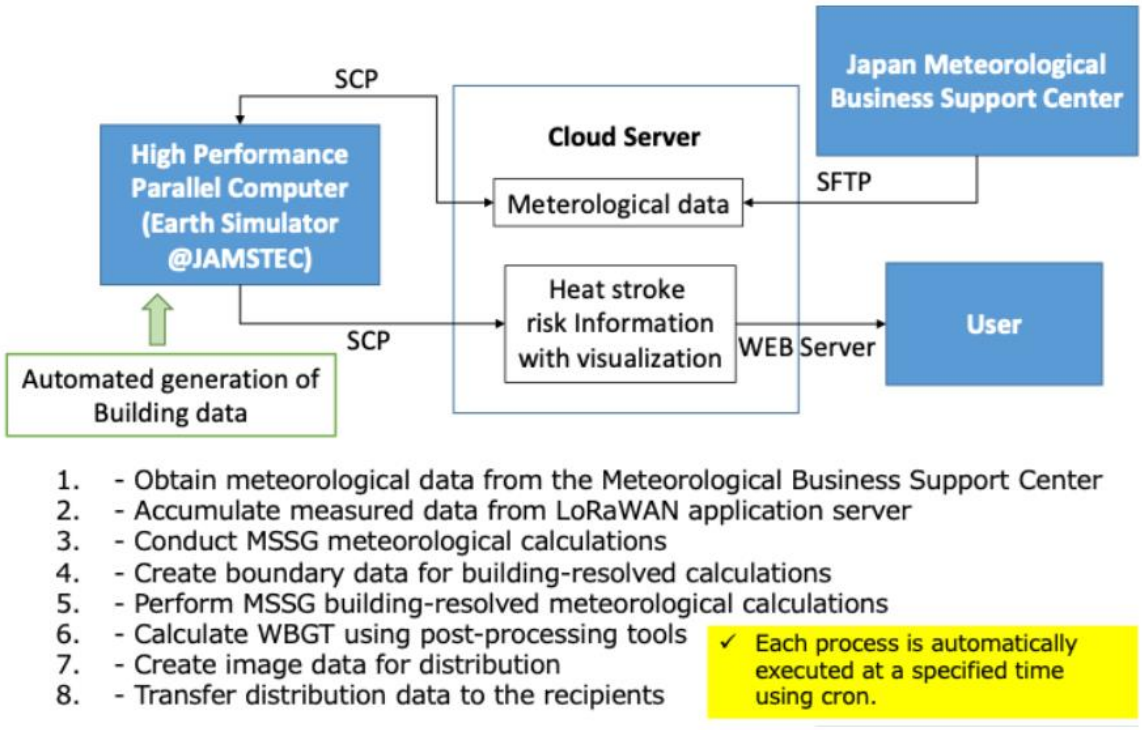


Figure 4. Automated system of data acquisition and computation.

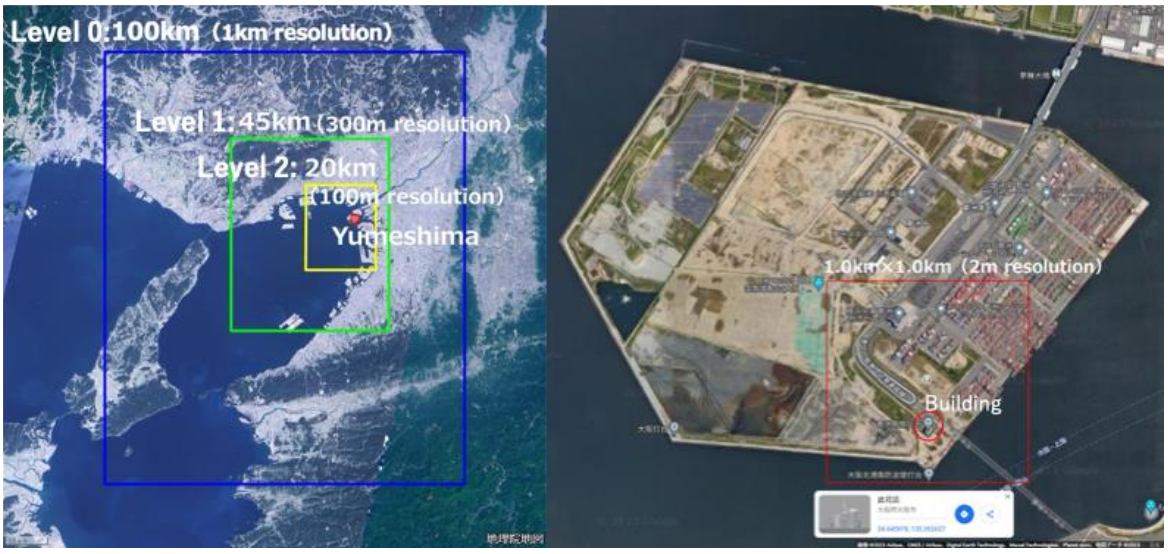


Figure 5. Three nested domains for mesoscale meteorological simulation (left) and the domain for micrometeorological simulation (right).

© ASCE

The measured data shows a gradual change, indicating a tendency to reflect the local meteorological conditions over time after the measurement instruments were installed at the locations. The comparison of temperatures shows that the calculated results eventually align well with the measurements. However, in the comparison of humidity, the calculated results tend to be about 10% lower than the measurements. Predicting low humidity results in a lower predicted risk of heatstroke, improvements are expected by further investigating the effects of evaporation over the ocean.

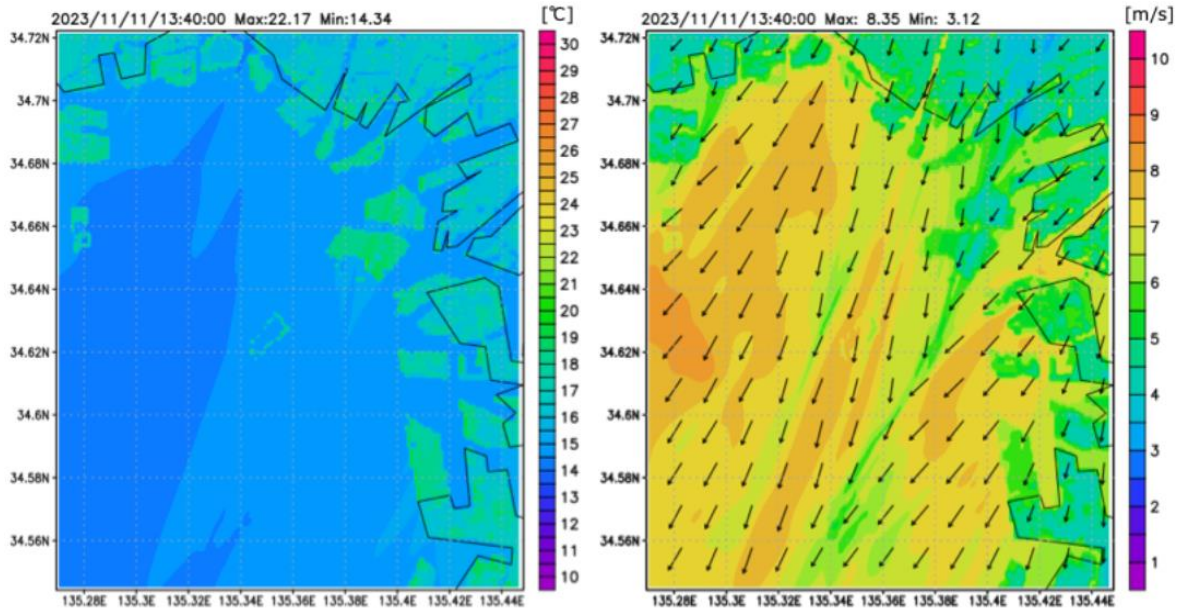


Figure 6. Temperature (left) and wind velocity (right) distributions obtained by the mesoscale meteorological simulation.

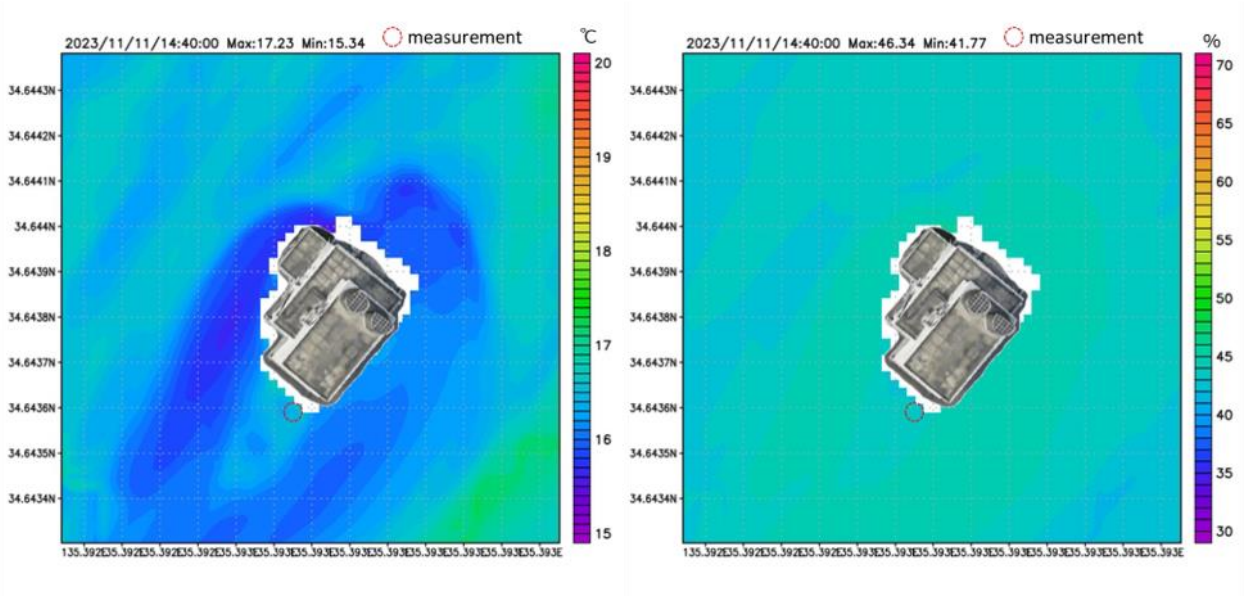


Figure 7. Temperature (left) and relative humidity (right) distributions in vicinity of the building shown in Figure 5 obtained by the micrometeorological simulation.

© ASCE

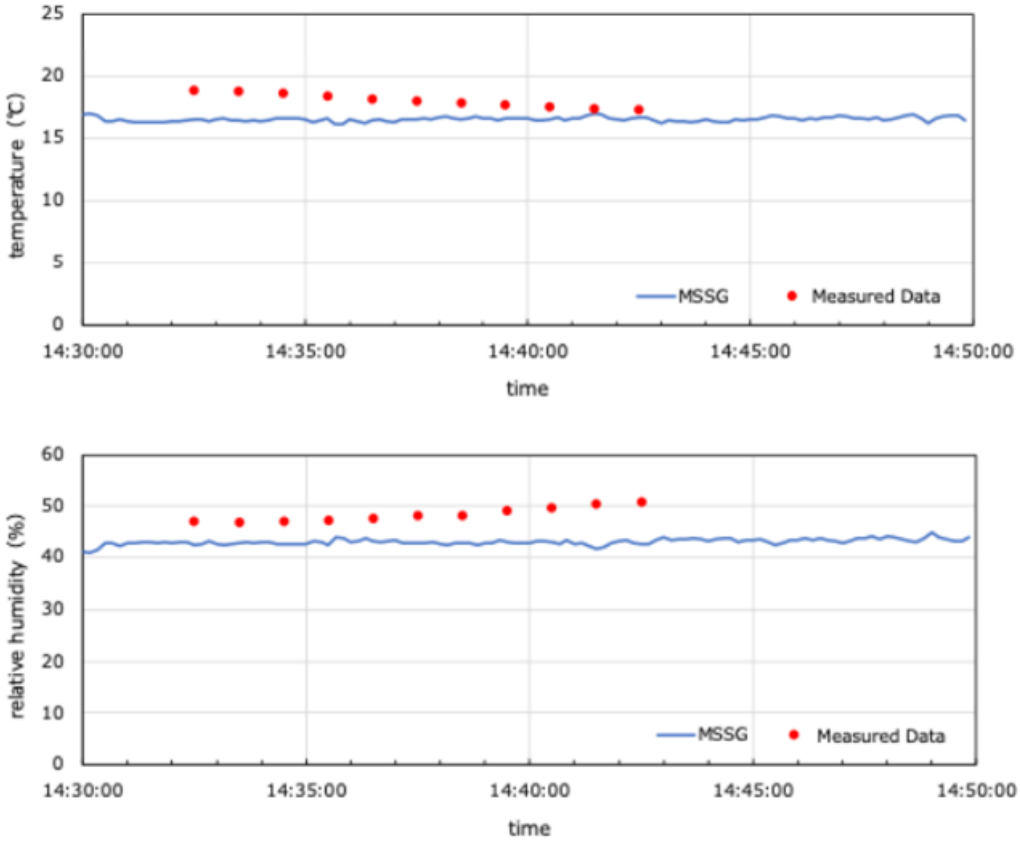


Figure. 8 Comparison of temperature (upper) and relative humidity (lower) between measurements and simulations.

CONCLUSION

We developed a method to automatically create digital twins from PLATEAU data and conducted micrometeorological analyses using this system. By comparing the results with measured data, such as temperature and humidity, we confirmed that the system accurately reproduces air temperature. It has become possible to automatically distribute heat index maps for event venues predicted by this system. At this stage, humans are responsible for assessing risks manually based on the predictions. As the next step, further contributions to heatstroke prevention are expected, such as expanding the system to enable automated decision-making through collaboration with AI. Additionally, to more faithfully reproduce the local micrometeorological conditions, we plan to perform data assimilation analysis using measurement data.

ACKNOWLEDGEMENTS

Part of this research was conducted as an activity under the Strategic Innovation Promotion Program (SIP) Phase 3, "Development of a Smart Infrastructure Management System" (JPJ012187, Research Promotion Organization: Public Works Research Institute), led by the Cabinet Office Council for Science, Technology, and Innovation.

© ASCE

REFERENCES

Japan Meteorological Agency. (2024). Climate Change Monitoring Report 2023, https://www.jma.go.jp/jma/en/NMHS/ccmr/ccmr2023.pdf.

LoRa Alliance. (2020). TS001-1.0.4 LoRaWAN® L2 1.0.4 Specification, https://resources.lora-alliance.org/technical-specifications/ts001-1-0-4-lorawan-l2-1-0-4-specification.

Onishi, R., Sugiyama, D., and Matsuda, K. (2019). "Super-Resolution Simulation for Real-Time Prediction of Urban Micrometeorology" *SOLA*, 15, 178−182.

O-Tani, H., Iiyama, K., Takaya, S., and Yabe, M. (2022). "Automated Model Construction of Urban Structures with Limited Digital Data" *Journal of Earthquake and Tsunami*, 16(3), 2240004.

© ASCE

Quantitative Evaluation Methods of Ash and Cement Concrete Powder:CO_2 Fixation Reactions

Shun Kawabe[1]; Haruya Suzuki[2]; Sota Murase[3]; Hideo Komine[4]; and Daichi Ito, Dr.Eng.[5]

[1]Dept. of Civil and Environmental Engineering, Waseda Univ., Tokyo, Japan.
Email: skawabe@asagi.waseda.jp
[2]Dept. of Civil and Environmental Engineering, Waseda Univ., Tokyo, Japan.
Email: suzuharu@moegi.waseda.jp
[3]Dept. of Civil and Environmental Engineering, Waseda Univ., Tokyo, Japan.
Email: murase_s@toki.waseda.jp
[4]Professor, Faculty of Science and Engineering, Dept. of Civil and Environmental Engineering, Waseda Univ., Tokyo, Japan. Email: hkomine@waseda.jp
[5]Dept. of Urban and Civil Engineering, College of Engineering, Ibaraki Univ., Ibaraki, Japan.
Email: daichi.ito.ev17@vc.ibaraki.ac.jp

ABSTRACT

The increase in extreme weather is considered to be caused by global warming resulting from the increase in emitted greenhouse gases such as CO_2. To reduce the net amount of CO_2 emitted, CO_2 fixation with by-products and cement concrete is considered. There are various studies about quantitative evaluation methods of the amount of CO_2 fixated. However, there are few studies examining whether the method can be used equally for various types of samples or its accuracy. In this study, CO_2 was fixed in two types of incineration fly ash, cement concrete powder, and a simulated sample, and quantitative evaluation was performed by four methods and compared. The results of this study confirmed that the samples used in this study have CO_2 fixation capacities and that CO_2 mass balance method, carbonate content test method, and Thermogravimetry-Differential Thermal Analysis coupled with Mass Spectrometry (TG-DTA-MS) method showed similar values, which seemed correct, of the amount of CO_2 fixation, while Fourier transform infrared spectroscopy (FTIR) method showed larger values.

INTRODUCTION

Currently, extreme weather such as rising sea levels, unprecedented heavy rains, and droughts is reported all over the world. One of the reasons of them is considered to be global warming. In Japan, Carbon dioxide (CO_2) accounts for approximately 90% of greenhouse gases emitted, and CO_2 emitted worldwide has contributed to 76% of global warming since the industrial revolution (Japan Center for Climate Change Actions 2022). Thus, reducing the net amount of CO_2 emitted is considered important to prevent extreme weather and global warming.

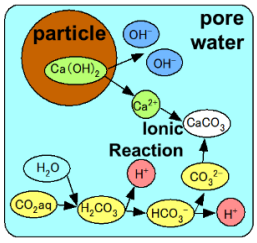
The authors' research group focus on the CO_2 fixation reaction with by-products (Komine et al. 2023a, b; Umino et al. 2014, 2017). Figure 1 is the overview of the CO_2 fixation reaction. Some by-products contain calcium (Ca), as compounds such as calcium hydroxide ($Ca(OH)_2$). Calcium ion (Ca^{2+}) dissolves in pore water from the particles of the by-products. Carbonate ion (CO_3^{2-}) also dissolves in the pore water from the atmosphere. Then Ca^{2+} and CO_3^{2-} form calcium carbonate ($CaCO_3$) by ionic reaction. This reaction occurs even under normal temperature and normal pressure conditions, and $CaCO_3$ produced in this reaction is thermodynamically stable.

© ASCE

So, it is known that the CO_2 fixation reaction with by-products can fix atmospheric CO_2 in a stable state by only using low energy and cost.

In order to introduce the CO_2 fixation reaction into the social system, appropriate methods for quantitatively evaluating the amount of CO_2 fixation are essential. There are many studies using quantitative evaluation methods for the amount of CO_2 fixation. For example, the method by calculating CO_2 mass balance in the CO_2 fixation test (Komine et al. 2023a, b; Umino et al. 2014, 2017) and the method by calculating data in the carbonate content test (Umino et al. 2014, 2017), the method using Thermogravimetry-Differential Thermal Analysis coupled with Mass Spectrometry (TG-DTA-MS) (Asano et al. 2023; Ashraf et al. 2015; Chen et al. 2016; Jang, Lee 2016; Moon, Choi 2019; Sakamoto et al. 2023; Zhan et al. 2019), and the method using Fourier transform infrared spectroscopy (FTIR) (Ashraf et al. 2015) have been used in the CO_2 fixation research. However, the samples used in these previous studies are limited, such as only cement concrete or only slag. Also, these studies used only one or two quantitative evaluation methods. In other words, there are few studies that compare various types of samples and various quantitative evaluation methods.

To examine the accuracy of the various methods and whether they can be used equally, this study tested the four evaluation methods on four different samples. The four methods were the CO_2 mass balance, carbonate content test, TG-DTA-MS, and FTIR which was found to be able to be used for the quantitative evaluation of one incineration fly ash (Kawabe et al. 2024). In this study, to confirm whether similar results could be obtained for various types of samples and to verify their accuracy, four samples were tested being: two types of incineration fly ash (FC_K, GBf), cement concrete powder (CKR02), and a simulated sample (IdSP), and the results of quantitative evaluation methods by CO_2 mass balance method, carbonate content test, TG-DTA-MS, and FTIR were compared.



$$CaO + H_2O \rightleftarrows Ca(OH)_2$$
$$Ca(OH)_2 \leftrightarrows Ca^{2+} + 2OH^-$$
$$CO_2 + H_2O \rightleftarrows H_2CO_3$$
$$H_2CO_3 \rightleftarrows HCO_3^- + H^+$$
$$HCO_3^- \rightleftarrows CO_3^{2-} + H^+$$
$$Ca^{2+} + CO_3^{2-} \rightleftarrows CaCO_3$$

Figure 1. Overview of CO_2 Fixation Reaction

MATERIALS

Four different samples which were sieved to remove particles larger than 2 mm were used in this study. The fundamental characteristics of them are shown in Table 1. Water content during storage was measured by JIS A 1203:2020, particle density was measured by JIS A 1202:2020, and pH during storage was measured by JGS 0211-2020. In addition, the mass ratio of Ca was confirmed by X-ray fluorescence analysis (XRF), and the main mineral composition before and after the CO_2 fixation reaction was confirmed by powder X-ray diffraction (XRD).

The first sample is soot and dust FC_K. FC_K is the incineration fly ash of industrial waste generated when waste materials (cellulose, PP, PE) made from food packaging bags, wastewater treatment sludge (organic sludge, inorganic sludge), etc. are incinerated using RPF as fixed fuel. After collecting from an incinerator, it is subjected to chelation treatment.

© ASCE

The second sample is soot and dust GBf. GBf is the incineration fly ash of general waste generated by municipality that the authors named B. It is also subjected to chelation treatment.

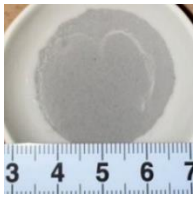
The third sample is cement concrete powder CKR02. CKR02 is made into a powder from a concrete test specimen using a compression test machine and a crusher.

The final sample is simulated sample IdSP. IdSP is a sample made to simulate FC_K. It is made by mixing calcium hydroxide reagent ($Ca(OH)_2$) and silica powder mainly composed of silicon dioxide (SiO_2) so that the mass ratio of Ca was approximately 30%.

METHODS

The experimental flow of this study is shown in Figure 2. Firstly, CO_2 was fixed in water content adjusted samples using the Constant Flow Aeration Type CO_2 Fixation Test (Komine *et al*. 2023a, b; Umino *et al*. 2014, 2017) shown in Figure 3. The test was stopped at various times to investigate if the evaluation method could be applied for samples with incomplete CO_2 fixation. Then the taken-out samples were oven dried and were tested with the evaluation methods explain later.

Table 1. Fundamental properties of samples

	Soot and dust, FC_K	Soot and dust, GBf	Cement concrete, CKR02	Simulated sample, IdSP
Photo				
Water Content during storage [%]	24.3	17.8	4.2	0.0
Particle Density [Mg/m^3]	2.84	2.59	2.72	2.40
pH during storage [-]	12.6	12.0	12.5	12.8
Ca Content [mass%]	30.7	20.0	12.0	33.7
Main Mineral Composition Before (Upper) and After (Bottom) CO_2 Fixation	$Ca(OH)_2$, $Ca_2Al[AlSiO_7]$	$Ca(OH)_2$, NaCl, KCl, CaClOH	$Ca(OH)_2$, SiO_2, $CaCO_3$, $CaAl_2(SiO4)_2$	$Ca(OH)_2$, SiO_2
	$CaCO_3$, $Ca_2Al[AlSiO_7]$	$CaCO_3$, NaCl, KCl, CaClOH	$CaCO_3$, SiO_2, $CaAl_2(SiO4)_2$	$CaCO_3$, SiO_2

In the CO_2 fixation test, the air passed through the specimen at a constant flow rate, and the CO_2 concentrations and temperatures of the air before and after passing through the specimen were measured. The testing condition of the CO_2 fixation test is shown in Table 2. As this study focuses on the accuracy of the four evaluation methods and as the evaluation methods are all

© ASCE

conducted for each experimental case, the difference in experimental conditions between sample types were not considered.

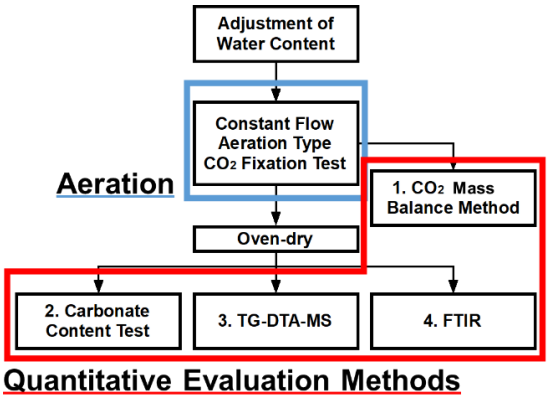


Figure 2. Flow Chart of This Study

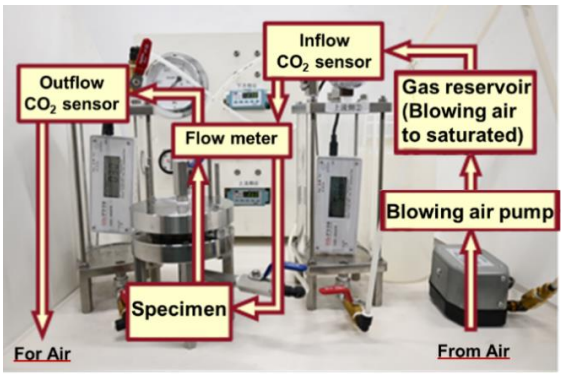


Figure 3. Apparatus of Constant Flow Aeration Type CO_2 Fixation Test

The testing procedure of the four evaluation methods are as follows:

The first method is the CO_2 mass balance method (Komine et al. 2023a, b; Umino et al. 2014, 2017). During the CO_2 fixation test, excess CO_2 was recorded at the inlet and outlet, and it was assumed that the difference in the CO_2 amount at the inlet and outlet would show the amount of fixated CO_2 in the specimen. The amount of CO_2 molecules at each minute in the inlet (n_{in}) and outlet (n_{out}) was calculated with the CO_2 concentration and temperature recorded in the Constant Flow Aeration Type CO_2 Fixation Test. Then the CO_2 fixation amount per unit mass ($m_{\mathrm{CO_2-sample}}$) was calculated using Eq. 1.

Table 2. Test Condition of the CO_2 Fixation Test

	FC_K	GBf	CKR02	IdSP
Water Content before aeration [%]	30	30	10	10
Specimen Dry Density [Mg/m^3]	0.53	0.78	1.0	0.53
Specimen Size [mm]	Φ 75, H 20	Φ 20, H 20	Φ 20, H 20	Φ 75, H 20
Flow Rate [L/min]	2	0.5	0.5	2

© ASCE

$$m_{\mathrm{CO_2-sample}} = \frac{M_{\mathrm{CO_2}}}{m_{\mathrm{s}}} \times \sum_{t=0}^{t_{\mathrm{end}}} (n_{\mathrm{in}}|_t - n_{\mathrm{out}}|_t) \quad (1)$$

Where, $m_{\mathrm{CO_2-sample}}$ [g-CO_2 / g-sample] is the amount of CO_2 fixation per unit mass; $M_{\mathrm{CO_2}}$ [g / mol] is the molar mass of CO_2; m_{s} [g] is the dry mass of specimen; t [min] is the elapsed time from start test; and t_{end} [min] is the elapsed time t at stop the CO_2 fixation test; n_{in}, n_{out} [mol] are the amounts of CO_2 flowing in, and out at each minute.

The second method is the carbonate content test method (Fukue et al. 2000; Umino et al. 2014, 2017). The apparatus of this method is shown in Figure 4. In the carbonate content test, oven dried samples were reacted with hydrochloric acid (HCl) to generate CO_2 gas and the exhibited pressure from the gas was recorded. With the maximum pressure recorded (P_{max}), the $CaCO_3$ amount ($m_{\mathrm{CaCO_3}}$) was calculated by using a standard curve equation shown in Eq. 2 which was created using $CaCO_3$ reagents.

$$m_{\mathrm{CaCO_3}} = (0.0044\ \mathrm{g \cdot kPa^{-1}}) \times P_{\mathrm{max}} \quad (2)$$

Where $m_{\mathrm{CaCO_3}}$ [g] is the amount of $CaCO_3$; and P_{max} [kPa] is the maximum pressure in the acrylic reactor. The $CaCO_3$ amount per unit mass was calculated by dividing $m_{\mathrm{CaCO_3}}$ with the dry mass of the tested sample. The $CaCO_3$ amount per unit mass was obtained for the taken-out sample ($m^{\mathrm{after}}_{\mathrm{CaCO_3-sample}}$) and the sample at the initial state ($m^{\mathrm{before}}_{\mathrm{CaCO_3-sample}}$). Then the CO_2 fixation per unit mass was calculated using Eq. 3.

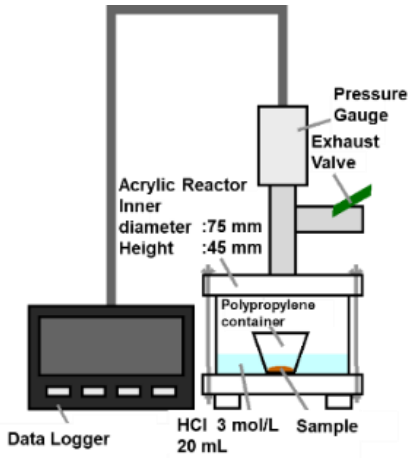


Figure 4. Apparatus of Carbonate Content Test

$$m_{\mathrm{CO_2-sample}} = \frac{M_{\mathrm{CO_2}}}{M_{\mathrm{CaCO_3}}} \times \left(m^{\mathrm{after}}_{\mathrm{CaCO_3-sample}} - m^{\mathrm{before}}_{\mathrm{CaCO_3-sample}}\right) \quad (3)$$

Where, $m_{\mathrm{CO_2-sample}}$ [g-CO_2 / g-sample] is the amount of CO_2 fixation per unit mass; $M_{\mathrm{CO_2}}$ [g / mol] is the molar mass of CO_2; $M_{\mathrm{CaCO_3}}$ [g / mol] is the molar mass of $CaCO_3$; and $m^{\mathrm{before}}_{\mathrm{CaCO_3-sample}}$, $m^{\mathrm{after}}_{\mathrm{CaCO_3-sample}}$ [g-$CaCO_3$ / g-sample] are the amounts of $CaCO_3$ per unit mass about initial (before), and taken-out (after) sample.

© ASCE

The third method is TG-DTA-MS method. TG-DTA-MS method, which is a combination of three tests, conducts pyrolysis on the sample for a certain temperature range (room temperature to 1000℃) and measures the mass loss (TG), the type of thermal event (DTA), and emitted gas mass spectrometry (MS). As mass loss measured in TG may be caused by other factors such as dehydration (Zhan et al. 2019), this study assumes that the temperature range in which CO_2 emissions are observed by MS, which is suggested to be reliable in identifying mass loss by CO_2 gas emissions (Chen et al. 2016), would be the range that $CaCO_3$ pyrolyze and emit CO_2 gas. Thus, the temperature range in which CO_2 is emitted was determined using MS and the mass loss at the determined range was assumed as the amount of CO_2 in the tested sample. The result of MS in this study is shown in Figure 5, and the determined temperature range is shown as a dashed line. TG-DTA-MS was conducted for the initial and taken-out sample and the CO2 fixation per unit mass was calculated using Eq. 4.

$$m_{\mathrm{CO_2-sample}} = m^{\mathrm{after}}_{\mathrm{CO_2-sample}} - m^{\mathrm{before}}_{\mathrm{CO_2-sample}} \tag{4}$$

Where $m_{\mathrm{CO_2-sample}}$ [g-CO_2 / g-sample] is the amount of CO_2 fixation per unit mass; $m^{\mathrm{after}}_{\mathrm{CO_2-sample}}$, $m^{\mathrm{before}}_{\mathrm{CO_2-sample}}$ [g-CO_2 / g-sample] are the amounts of CO_2 per unit mass about initial (before), and taken-out (after) sample, which are calculated by dividing the mass loss (TG) with dry mass.

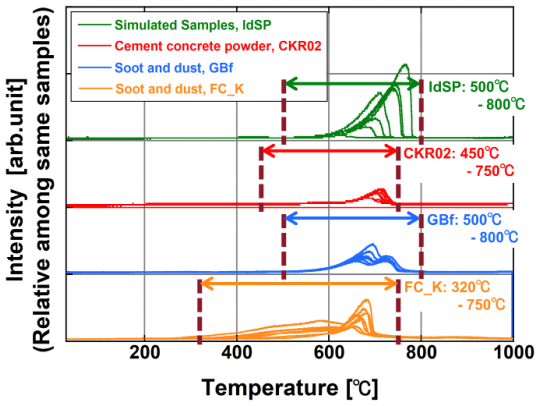


Figure 5. Result of MS and temperature range (mass to charge ratio m/z is 44 means CO_2)

The final method is the FTIR method. FTIR method used the property that samples absorb infrared light at a specific wavelength to calculate $CaCO_3$ amount. The Attenuated Total Reflection (ATR) method, which is a type if measurement method of FTIR, is shown as a conceptual illustration in Figure 6. The test was conducted three times and the reflectance (R) was measured. To correct baseline shifts, the results were normalized to $NDSI$ (Normalized Difference Spectral Index) (Inoue et al. 2008) using Eq. 5, and $NDSI$ were averaged. The averaged $NDSI$ was converted to absorbance (A) using Eq. 6. methods for calculating $NDSI$ are shown as Eq. 5 and 6.

$$NDSI = \frac{R - R_{2700}}{R + R_{2700}} \tag{5}$$

© ASCE

$$A = \log_{10}\left(\frac{1-NDSI}{1+NDSI}\right) \quad (6)$$

Where, $NDSI$ [-] is the Normalized Difference Spectral Index; R [%] is the reflectance of infrared lights collected in the test; R_{2700} [%] is R at 2700 cm^{-1} where absorbance is considered to be zero; and A [-] is absorbance. According to Beer's law, A is proportional to the molecular concentration (Furukawa 2018). In this study, the CaCO3 amount of the sample was calculated using the maximum of A ($A_{\max}$) in the wavenumber region of 1350 cm^{-1} to 1500 cm^{-1}, which is the maximum A among the obtained peaks that represents $CaCO_3$ and represents the stretching vibration of the C-O bonds (Saeki et al. 2022). Before conducting FTIR, a standard curve was created using $CaCO_3$ reagents and silica powder to obtain Eq. 7.

$$C_{CO_2} = 2.4898 \times A_{\max} \quad (7)$$

Where C_{CO_2} [g-CO_2 / g-sample] is the CO_2 concentration in sample; and $A_{\max}$ [-] is the maximum value of absorbance A between 1350 cm^{-1} and 1500 cm^{-1}. Using Eq. 7, C_{CO_2} was calculated with $A_{\max}$. Since C_{CO_2} can be regarded as $m^{\text{before}}_{CO_2-\text{sample}}$ or $m^{\text{after}}_{CO_2-\text{sample}}$, the amount of CO_2 fixation per unit mass was calculated using Eq. 4.

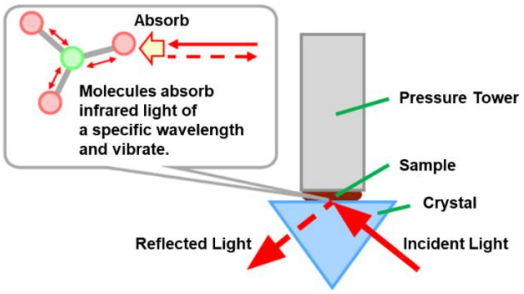


Figure 6. Image of FTIR (ATR)

RESULT AND DISCUSSION

The relation between the CO_2 fixation reaction progression $n_{\text{out}}/n_{\text{in}}$ when the CO_2 fixation test was stopped and the amount of CO_2 fixation per unit mass $m_{CO_2-\text{sample}}$ is shown in Figure 7. It could be seen that there was a positive correction between $n_{\text{out}}/n_{\text{in}}$ and $m_{CO_2-\text{sample}}$ for all cases except for the case of GBf tested with FTIR. Which indicates that all four samples have CO_2 fixation capability, and it was suggested that the amount of CO_2 fixation can be evaluated by the four methods. The quantitative evaluation methods by CO_2 mass balance, carbonate content test, and TG-DTA-MS showed similar $m_{CO_2-\text{sample}}$ values while FTIR showed significantly larger $m_{CO_2-\text{sample}}$ values. From which, it was considered that the amounts of CO_2 measured by methods other than FTIR may show a closer CO_2 fixation amount to the true value.

Additionally, FTIR cases showed large deviations which was considered to be caused by the limited applications of FTIR (ATR) for solid samples. Beer's law, which is a basic law used in the FTIR method, is typically applied to gases and dilute solutions (Furukawa 2018), and the infrared lights are known to be disoriented by the multiple reflection on the particle surface in

© ASCE

powder samples (Ozaki 2019). In fact, it could be also observed that GBf case, which has fairly larger particles (Table 1), had the large scattering, while the other samples, which have finer particles, had large values than other methods. From which, it could be suggested that the particle size may have strong influence on the value of the FTIR method, supporting the previous consideration. As FTIR cases show positive correlation between $n_{\mathrm{out}}/n_{\mathrm{in}}$ and $m_{\mathrm{CO_2-sample}}$, it was considered that the values by FTIR may be corrected by applying the diffuse reflection method and the Kubellka-Munk equation (Ochiai 2010, Hattori et al 1981).

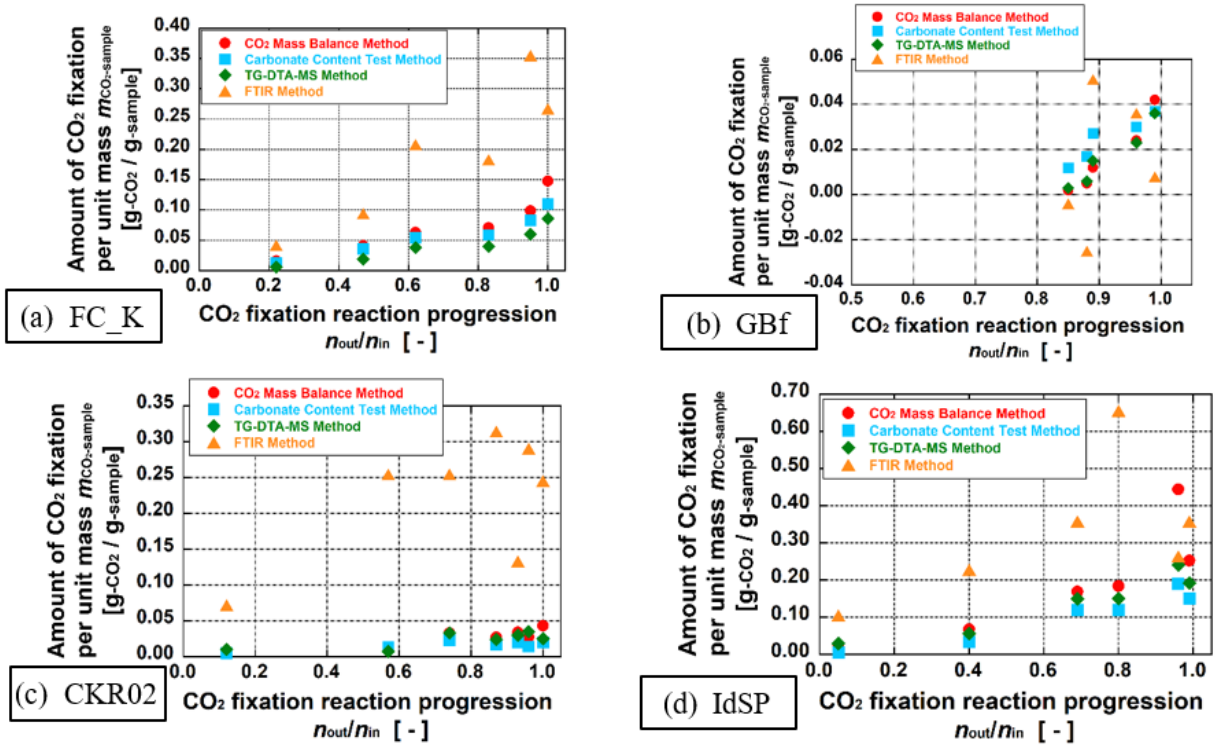


Figure 7. Comparison of four methods ((a): Soot and dust, FC_K, (b): Soot and dust, GBf, (c): Cement concrete powder, CKR02, and (d): Simulated sample, IdSP)

CONCLUSION

In this study, CO_2 fixation tests were conducted for two types of incineration fly ash (FC_K, GBf), cement concrete powder (CKR02), and simulated sample (IdSP). The samples were then quantitatively evaluated by four methods, CO_2 mass balance method, carbonate content test method, TG-DTA-MS method, and FTIR method, and the methods were compared. It was found that for most cases CO_2 fixation reaction progression $n_{\mathrm{out}}/n_{\mathrm{in}}$ and the amount of CO_2 fixation per unit mass $m_{\mathrm{CO_2-sample}}$ showed positive correlations indicating that it is suggested that the CO_2 fixation amount can be evaluated by four evaluation methods. The CO_2 mass balance method, the carbonate content test method, and the TG-DTA-MS method showed similar values suggesting that these values may show values close to the true CO_2 fixation amount. While the FTIR method showed large deviations, suggesting that further corrections may be needed to make it applicable.

© ASCE

ACKNOWLEDGEMENTS

Part of the experiments and interpretation of the results of this study were supported by Japan Institute of Country-ology, Engineering and The Geo-Kagaku Center, and were cooperated by Tokoro lab in Waseda Univ. Also, This work was the result of using research equipment's (RINT-Ultima III, ZSX Primus II, Thermo Mass Photo, and Nicolet 6700: Material Characterization Central Laboratory) shared in MEXT Project for promoting public utilization of advanced research infrastructure (Program for supporting construction of core facilities) Grant Number JPMXS0440500024. Furthermore, some of samples were given by MIDAC Holdings Co., Ltd and Kajima Road Co., Ltd. Generous advice on English writing was received from Dr. Eng. Ruan and Mr. Urano in Waseda University. The authors would like to express their deepest gratitude to them.

REFERENCES

Asano, Y., Yoshida, N., Mori, T., and Atarashi, D. 2023. "Carbonation mechanism of γ-C_2S-containing additive and influence of relative humidity on carbonation reaction". *Cement Science and Concrete Technology*. Vol. 77. pp. 508-515.

Ashraf, W., Olek, J., and Atakan, V. 2015. "A Comparative Study of the Reactivity of Calcium Silicates during Hydration and Carbonation Reactions". *14th International Congress on the Chemistry of Cement (ICCC 2015).*

Chen, K.-W., Pan, S.-Y., Chen, C.-T., Chen, Y.-H., and Chiang, P.-C. 2016. "High-gravity carbonation of basic oxygen furnace slag for CO_2 fixation and utilization in blended cement". *Journal of Cleaner Production.* Vol. 124. pp. 350-360.

Fukue, M., Kato, Y., Nakamura, T., and Moriyama, N. 2000. "A Method for Determining Carbonate Content for Soil sand Evaluation of the Results". *Soil mechanics and foundation engineering.* Vol. 49. No. 2. pp. 9-12.

Furukawa, Y. 2018. *Infrared Spectroscopy*. Kodansha. 306p. ISBN 978-4-06-156904-1.

Hattori, T., Shirai, K., Niwa, M., and Murakami, Y. 1981. "Quantitative Interpretation of Infrared Diffuse Reflectance Spectra over Whole Concentration Range". *Bulletin of the Chemical Society of Japan.* Vol. 54. No. 7. pp. 1964-1967.

Inoue, Y., Miah, G., Sakaiya, E., Nakano, K., and Kawamura, K. 2008. "NDSI Map and IPLS Using Hyperspectral Data for Assessment of Plant and Ecosystem Variables – With a Case Study on Remote Sensing of Grain Protein Content, Chlorophyll Content and Biomass in Rise –". *Journal of The Remote Sensing Society of Japan.* Vol. 28. No. 4. pp. 317-330.

Jang, J. G., and Lee, H. K. 2016. "Microstructural densification and CO_2 uptake promoted by the carbonation curing of belite-rich Portland cement". *Cement and Concrete Research.* Vol. 82. pp. 50-57.

Japan Center for Climate Change Actions. 2022. "Greenhouse gas emissions in data (Japan)". <https://www.jccca.org/global-warming/knowleadge05>(Jan. 15, 2024). (Title translated by the author).

Kawabe, S., Suzuki, H., Murase, S., Komine, H., and Ito, D. 2024. "Comparison of the quantitative evaluation methods of CO_2 fixation reaction of industrial by-products for a carbon neutral society". *Journal of JGS.* Vol. 72. No. 9. pp. 40-44.

© ASCE

Komine, H., Saito, Y., and Suzuki, K. 2023a. “Experimental evaluation of carbon-capture properties of industrial by-products for post-carbon society”. *9th International Congress on Environmental Geotechnics*. pp. 325-332.

Komine, H., Yokoi, K., Taga, H., Saito, Y., and Suzuki, K. 2023b. “Fundamental study on the creation of carbon capture urban environment using CO_2 fixation materials”. *Journal of Japan Society of Civil Engineers.* Vol. 79. No. 1.

Moon, E.-J., and Choi, Y. C. 2019. “Carbon dioxide fixation via accelerated carbonation of cement-based materials: Potential for construction materials applications”. *Construction and Building Materials.* Vol. 199. pp. 676-687.

Ochiai, S. 2010. “Experimental Infrared Spectroscopy Fundamentals and Practical Methods 8. Diffuse Reflection Measurements”. *Journal of the Spectroscopical Society of Japan.* Vol. 59.No. 6. pp. 291-295.

Ozaki, Y. *Near-Infrared Spectroscopy*. Kodansha. 286p. ISBN 978-4-06-156902-7.

Saeki, N., Kurihara, R., and Maruyama, I. 2022. “Effect of RH on Carbonation of Hardened Cement Paste Particles Under General Atmospheric CO_2 Concentration Studied by FTIR Spectroscopy”. *Cement Science and Concrete Technology.* Vol. 76. pp. 36-44.

Sakamoto, W., Yoshida, N., Nishioka, Y., and Atarashi, D. 2023. “Effect of Chemical Reaction Between Calcium Carbonate and Silica Gel on the Thermal Decomposition of Carbonated C-S-H”. *Cement Science and Concrete Technology.* Vol. 77. pp. 459-466. (in Japanese with English abstract).

Umino, M., Komine, H., Murakami, S., and Setoi, K. 2014. “Carbon Dioxide Fixation Properties and Mechanism of Steel Slag in the Use for Formation of Low-carbon Society”. *Japanese Geotechnical Journal.* Vol. 9. No. 4. pp. 469-478.

Umino, M., Komine, H., Murakami, S., Yasuhara, K., Setoi, K., and Watanabe, Y. 2017. “Iron and Steel Slag Properties and Mechanisms for Carbon Dioxide Fixation in a Low-carbon Society”. *Geotechnical Engineering Journal of the SEAGS & AGSSEA.* Vol. 48. No. 1. ISSN 0046-5828.

Zhan, B. J., Xuan, D. X., Poon, C. S., and Shi, C. J. 2019. “Mechanism for rapid hardening of cement pastes under coupled CO_2-water curing regime”. *Cement and Concrete Composites.* Vol. 97. pp. 78-88.

© ASCE